EUROPEAN SYNCHROTRON RADIATION FACILITY

INSTALLATION EUROPEENNE DE RAYONNEMENT SYNCHROTRON

ESRF

Long Term Project Report : Interim

Summary Page

Proposal Number: HC-1428

1. Beamtime Used

Please give a short summary of progress for each scheduling period for which beamtime has been allocated/used:

Scheduling period	Beamline(s) Used	Shifts Used	Summary of results obtained
2017 / II	ID28 DS@ID28	18	Lattice dynamics of $BaVS_3$ from IXS, paper in preparation
2017 / II	DS@ID28	6	Elasticity measurements of $SrSO_4$ from thermal diffuse scattering
2017 / II	DS@ID28	3	Lattice dynamics of Pb_2SnO_4 from TDS and ab initio calculations
2017 / II	ID28	18	Phonon dispersion measurements of calcite at high temperature in diamond chamber
2017 / I	ID28	18	F point softening of transverse acoustic phonon in calcite and magnesite at ambient and elevated temperatures
2017 / I	ID28	18	Lattice dynamics of WO_3

2. Resources Provided by User team (financial, personnel, technical...):

Personnel:
Up to April 2015: engineer (Luis Costa)
February 2015 – 30.06.2016: post doc (Dr. Thanh Tra Nguyen)
01.08.2016 – 30.06.2019: post doc (Dr. Adrien Girard)
01.03.2017 – 28.02.2018: PhD student (Michal Stekiel)

Financial:
Direct cash contribution: > 83.000 €

Other:
Work shop time in Frankfurt

3. **Technical and Scientific Milestones Achieved** (in relation to the milestones identified in the original proposal)**:**

Year 1
Components have been purchased and installed. Diffractometer has been set-up and has been integrated into ESRF IT infrastructure. Significant delays have been due to late delivery of mirrors by the ESRF. Start of final commissioning phase has been delayed due to problems with the vacuum system.

Year 2
Diffractometer and detector have been set-up and have been integrated into ESRF IT infrastructure. Diffractometer has been successfully commissioned. Measurement strategies have been refined. Software for instrument control, data collection and analysis has been developed. Sample environment for cooling and heating of the sample has been commissioned. Software suite for reduction of diffuse scattering data has been completed. Diffractometer has been opened for other users and included in the 2016/II call.
Fabrication of the HT diamond anvil cell has been severely delayed due to technical problems.

Phonon dispersion curves of iron carbonate in the diamond anvil cell have been measured with IXS. The elastic moduli were extracted in order to investigate the pressure-induced spin transition influence on the sound wave velocities.

Year 3
General user operation at DS@ID28 for rapid survey of reciprocal space for subsequent IXS experiments was successful for the following groups (see full reports by the respective groups):

- St Petersburg State Polytechnical University
  BURKOVSKIY Roman, ANDRONIKOVA Daria, KNIAZEVA Mariia
- Ioffe Physical-Technical Insitute
  BRONWALD Iurii, VAKHRUSHEV Sergey
- Swiss-Norwegian Beam Lines at ESRF
  CHERNYSHOV Dmitry, DOVGALYUK Yury
- Universitaet G H Siegen
  SIMONOV Arkadiy
- University of Oxford
  GOODWIN Andrew Leslie, YEUNG Hamish
- Tel Aviv University
  GORFMAN Semen
- CNRS UMR 6508 / ENSICAEN Laboratoire CRISMAT
  PAUTRAT Alain, DUVERGER-NEDELLEC Elen, PEREZ Olivier
- INP Grenoble - CNRS - UJF Laboratoire SIMAP

DE BOISSIEU Marc

- University of Edinburgh Centre for Science at Extreme Conditions
  LOA Ingo, ASTON James, FREEMAN Kenneth, MCMAHON Malcolm
- Krakow University of Science & Technology
  KOZLOWSKI Andrzej, BIALO Izabela, TABIS Wojciech
- CNRS - UJF - Institut Neel
  LORENZO Emilio, MONCEAU Pierre, RODIERE Pierre
- Stanford University Department of Applied Physics
  GREVEN Martin
- University of Minnesota School of Physics and Astronomy
  YU Biqiong
- NHMFL National High Magnetic Field Laboratory
  TOZER Stanley, CONIGLIO William, GROCKOWIAK Audrey
- European Commission Joint Research Centre Institute for Transuranium Elements
  CACIUFFO Roberto, LANDER Gerard, MAGNANI Nicola
- Universite de Geneve
  WEHINGER Bjorn
- Kurnakov Institute General & Inorganic Chemistry
  BOYTSOVA Olga
- Moscow State University Department of Materials Science
  ELISEEV Andrei, PETUKHOV Dmitrii
- Karlsruhe Institute of Technology Institut fuer Festkoerperphysik
  LE TACON Matthieu
- MPI Chemische Physik DRESDEN
  HICKS Clifford
- MPI fuer Festkoerperforschung STUTTGART
  KIM Hun-ho, MINOLA Matteo, LEFRANCOIS Emilie
- Helmholtz Zentrum Berlin
  FRITSCH Katharina, HABICHT Klaus
- Université de Montpellier Institut Charles Gerhardt
  PAULUS Werner
- Georg-August-University of Goettingen, Institut for Physical Chemistry
  MAITY Avishek
- University of South Florida Novel Materials Laboratory/Physics
  NOLAS George, WEI Kaya
- University of Copenhagen
  MADSEN Anders, KOVACIC Monika, SOVAGO Ioana
- Institut Laue-Langevin
  SCHMALZL Karin
- CEA Grenoble
  RAYMOND Stephane
- Forschungszentrum Juelich
  BINISKOS Nikolaos
- CNRS/UGA UPR2940 Institut Néel
  QUEMERAIS Pascal
- Inst. of Radioengineering & Electronics (RAS) MOSCOW
  SINCHENKO Alexander

- URA CNR 002 - Universite Paris-Sud 11 Laboratoire de Physique des Solides
  BELLEC Ewen, FOURY-LEYLEKIAN Pascale
- CNRS Laboratoire de Champs Magnetiques Intenses
  FAUGERAS Clément, MOLAS Maciej
- CNRS LNCMI
  POTEMSKI Marek

We used the combination of DS@ID28 and IXS experiments for benchmark experiments with Pb_2SnO_4, $BaVS_3$, WO_3, $SrSO_4$ and $CaCO_3$ at low and high temperatures

Commissioning experiments with the newly developed externally heated diamond anvil cell have been performed. Technical problems have been encountered and are currently being solved by the vendor. The cell is expected to be fully operational in the second quarter of 2018.

The performance of the diffractometer has been studied in great detail and a corresponding manuscript will be submitted soon.

4. List of publications directly resulting from beamtime used for this Long Term Project:

Stekiel, M., Nguyen-Thanh, T., Chariton, S., McCammon, C., Bosak, A., Morgenroth, W., Milman, V., Refson, K. and Winkler, B. (2017). High-pressure elasticity of $FeCO_3$-$MgCO_3$ carbonates. *PEPI*, 271, pp. 57-63.

Bosak, A. (2017) ID28 diffraction side station. Commissioning report. Unpublished

Nguyen-Thanh, T., Bosak, A., Bauer, J. D., Luchitskaia, R., Refson, K., Milman, V. and Winkler, B. (2016). Lattice dynamics and elasticity of $SrCO_3$. *Journal of Applied Crystallography*, *49*(6) 1982-1990.

Further publications in preparation :

Girard, A., Stekiel, M., Morgenroth, W., Bosak, A., Taniguchi, H. and Winkler, B., *A new diffractometer for diffuse scattering studies at the ID28 beamline of the ESRF.*

Stekiel, M., Girard, A., Nguyen-Thanh, T., Chariton, S., Morgenroth, W., Bosak, A., McCammon, C. and Winkler, B., *Lattice dynamics and F point softening in carbonates.*

Stekiel, M., Nguyen-Thanh, T., Morgenroth, W., Bosak, A. and Winkler, B., *Lattice dynamics of low temperature phases of WO_3.*

Girard, A., Ilakovac, V., Stekiel, M., Morgenroth, W., Bosak, A. and Winkler, B., *Soft phonon driven hexagonal-orthorhombic phase transition in $BaVS_3$.*

Girard, A., Stekiel, M., Morgenroth, W., Wehinger, B., Mirone, A., Bosak, A. and Winkler, B., *Elastic tensor of $SrSO_4$ from thermal diffuse scattering.*

Girard, A., Stekiel, M., Morgenroth, B., Bosak, A. and Winkler, B., *Lattice dynamics of Pb_2SnO_4 from combined TDS, IXS and DFT calculations.*

Start of report in free format

Summary of diffuse scattering experiments carried out with ID28 side station.

1. Elasticity measurements from thermal diffuse scattering.

The elasticity tensor, i.e. the full set of elastic stiffness coefficients, is the fundamental quantity required for the description of the elastic properties of crystalline materials. Accurate measurements of the elasticity tensor are a prerequisite for the interpretation of seismological observations, which provide insight into the composition, temperature and pressure of Earth's interior. In condensed matter physics, elastic properties are important in the study of phase transitions in systems with pronounced interaction of phonons with other quasi-particles. Such interaction may include electron-phonon coupling in superconductors or spin-phonon coupling in low dimensional spin systems.

Researchers from the University of Geneva, Paul Scherrer Institute and the ESRF have shown in their article published in Physical Review Letters that the full elasticity tensor can be determined by high-precision measurements of thermal diffuse scattering in a single crystal [B. Wehinger et al, PRL 118, 035502 (2017)]. Thermal diffuse scattering is due to the vibrations of atoms around their equilibrium positions. In the vicinity of Bragg reflections, the measured intensities are mainly due to scattering of x-rays by acoustic phonons and hence the elasticity tensor can be extracted by an analysis of the scattering intensities. In their paper, the investigated benchmark materials were high-quality single crystals of magnesium oxide and calcite. Here we show that ID28 side station can be used to carry out similar surveys of elastic properties.

We have investigated elastic stiffness coefficients of a natural single crystal of strontium sulfate $SrSO_4$. During measurements, the sample is rotated in small angular steps of only 0.1 degrees with 1 second exposure times, in order to accurately measure the weak diffuse scattering. Measurements were taken at various temperatures. The data treatment required the adaption of a novel analysis technique and the development of an appropriate software package, which allows the precise reconstruction of diffuse scattering. The software simultaneously fits approximately 40 individual intensity data by taking into account the exact scattering geometry and symmetry of the crystal. The full formalism of the fitting procedure will be described in detail in a forthcoming publication (Girard, A., Stekiel, M., Morgenroth, W., Wehinger, B., Mirone, A., Bosak, A. and Winkler, B., *Elastic tensor of $SrSO_4$ from thermal diffuse scattering. In prep.*).

We first considered the determination of the elastic constants from thermal diffuse scattering measured at a single temperature. For the fit, scattering intensities in the proximity of the 40 most intense Bragg reflections were considered. Experimental scattering intensities and calculated thermal diffuse scattering intensities from the fitted elastic constants are compared in Fig. 1, top panel for the 220 reflection. The corresponding c_{ij} are summarized in table 1 along with the values measured from ultrasound, values obtained from DFT calculations, and the experimental bulk modulus from high pressure diffraction measurements. Despite an apparent agreement of experimental and calculated scattering intensities, most of the obtained elastic coefficients strongly differ from the theoretical values. This is due to a strong elastic scattering (Huang scattering) arising from either disorder or bad surface state. The problem of Huang scattering in imperfect crystals can be overcome if measurements are taken at slightly different temperatures. This strategy further allows to separate the inelastic contribution from elastic scattering that show different temperature behaviors. The bottom panel of

Fig. 1 shows the calculated TDS and the subtraction of diffuse intensities measured at 90 K and 130 K. The corresponding c_{ij} are summarized in table 1. In particular, the bulk modulus derived from the elastic stiffness tensor agrees better with the result obtained by high pressure measurements and by DFT calculations, and the c_{ij} from the multi-temperature analysis are generally in good agreement with values obtained from ultrasound spectroscopy and/or DFT calculations.

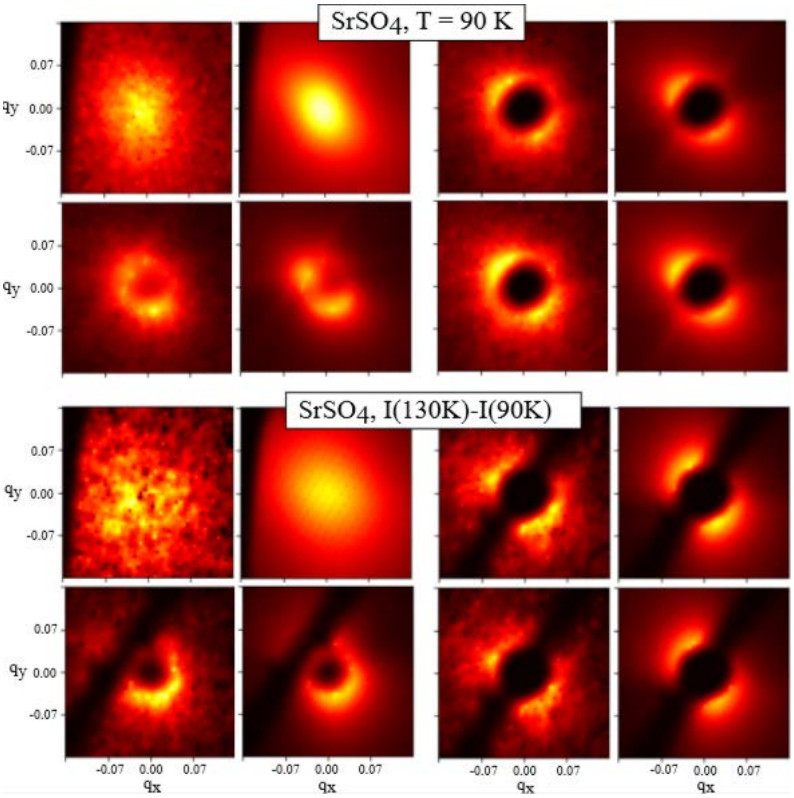

Figure 1: Experimentally determined diffuse scattering and calculated TDS of $SrSO_4$ 220 reflection with q ∈ [0.06, 0.15] at T = 90 K (top panels), and with the multi-temperature method at T = 90, 130 K (bottom panels). Each image shows a cross section of the reciprocal space in the neighborhood of the selected Bragg peak. The data are grouped by pairs, with the experimental and calculated intensity distributions on the left-hand and right-hand side, respectively. The scattering intensity is shown on a linear color scale from black (zero) to white (maximal intensity).

Cij (GPa)	DFT	Ultrasounds	TDS T=90K	TDS MT	High P
C11	107.0 ± 2.2	104	106	107	
C22	90.7 ± 4.3	106	77	93	
C33	116.0 ± 3.7	129	200	126	
C44	17.7 ± 1.0	13.5	34	18	
C55	41.0 ± 1.0	27.9	38	26	
C66	25.8 ± 3.0	26.6	9	25	
C12	41.6 ± 2.1	77	49	50	
C13	49.4 ± 1.8	60	77	45	
C23	35.0 ± 2.0	62	22	53	
K (GPa)	61.7±1.1	81.8	76	68	56

Table 1: Comparison of $SrSO_4$ elastic constants as obtained from DFT, ultrasound measurements, TDS single temperature method and TDS multi-temperature (MT) method. The experimental bulk modulus from high-pressure diffraction measurements is also reported.

Importantly, the analysis is model-free and provides values with a precision comparable to standard methods like ultrasound measurements by Brillouin scattering. The advantage over these methods is that the new approach can be applied to very small and opaque crystals of arbitrary shape and symmetry. The new method allows to measure the elastic properties together with the crystal structure under the same experimental conditions. It implies a broad applicability in material science, geophysics and in the study of sound wave anomalies due to fundamental interactions in condensed matter physics. The proposed methodology can be extended to measurements at extreme conditions such as high pressures, high or low temperatures or high magnetic fields. The application to high pressures is particularly interesting for the establishment of an absolute pressure scale in a single experiment. Temperature dependent studies are also possible. At very low temperatures the strategy is expected to work well and potentially very useful in the study of spin-lattice coupling. At temperatures relevant for geophysical processes absolute values can be obtained if the adiabatic bulk modulus is known.

2. Structure and lattice dynamics of Pb_2SnO_4.

The structure and lattice dynamics of synthetic single crystals of lead stannate were investigated by single crystal diffraction and thermal diffuse scattering. These studies follow our observation of a peak in DSC measurements, indicative of a weak first order transition at T = 340 K (see Fig. 2). We have recorded diffraction data at temperatures between 200 K and 500 K across this transition and refined the structure in order to understand the structural changes associated with this phase transition. The refined structure at T = 500 K is shown in Fig 2.A and B in *ab* and *bc* planes, and is isostructural to the ambient temperature structure. It consists of SnO_6 octahedrons and PbO_4 tetrahedrons arranged along the long *c* axis. PbO_4 tetrahedrons are highly distorted due to the presence of a stereochemically active lone electron pair on the Pb ion. We observed a small kink in the temperature dependence of the unit cell volume across the transition, thereby confirming the weak-first order character of the transition (Fig. 2D). No significant variations of the bond lengths were observed across the transition (Fig. 2E). However, we observed a kink in the temperature dependence of the anisotropic displacement parameter U_{11} of PbO1, PbO2 and Sn atoms (Fig. 2F) while the ADPs of the oxygen atoms seem unaffected by the transition (Fig. 2G).

We also investigated the diffuse scattering of lead stannate (Fig. 3). The reconstructions of reciprocal space sections in hk0, h0l and 0kl planes are presented and compared to calculations. A remarkable agreement is observed, indicating that the diffuse features are due to the inelastic scattering from the phonons. The good agreement can be also appreciated with 3D reconstructions of the experimental and calculated TDS intensities. In particular, hk0 and hk2 planes show the most rich thermal diffuse scattering signatures. Selected features will be further investigated by momentum resolved IXS. The diffuse patterns observed in hk0 and hk2 planes originate from a soft transverse acoustic branch, which is related to the instability of the corner-sharing SnO_6 and edge-sharing PbO_4 chains against shear stress. We observed no change in the TDS across the transition at 340 K.

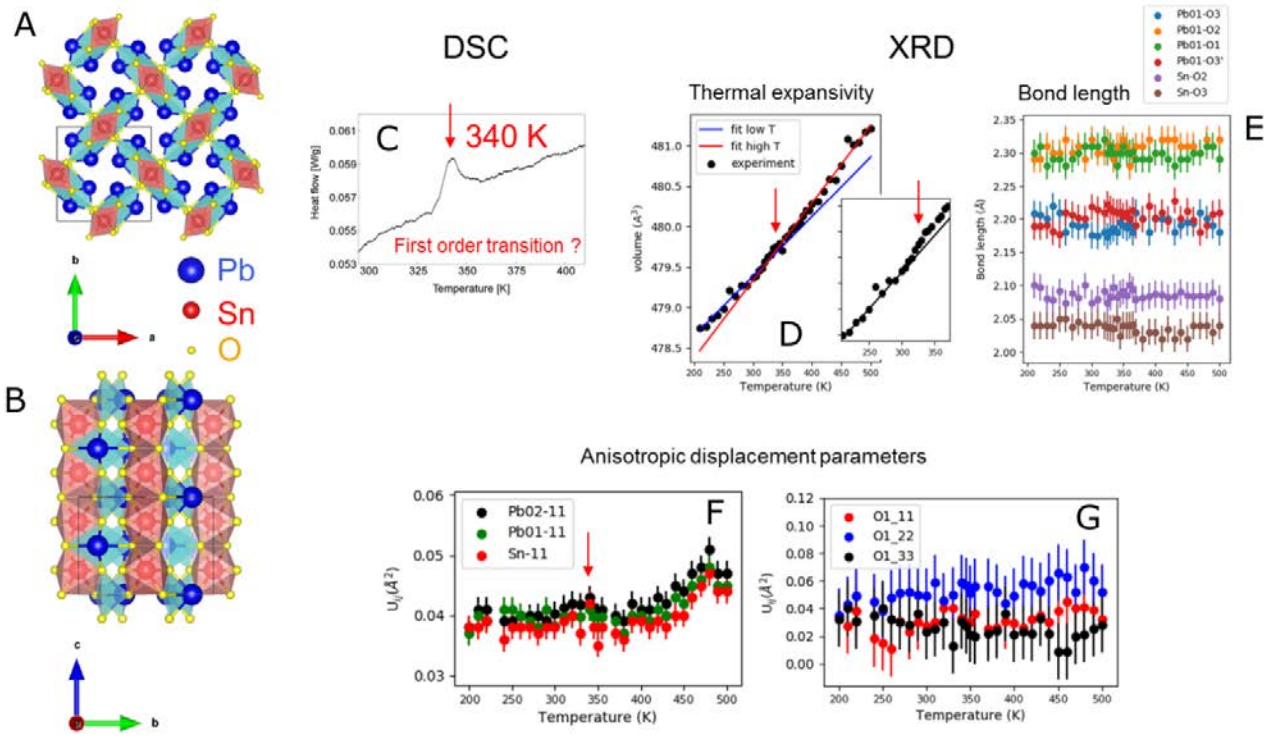

Figure 2: Structure of lead stannate in *ab* (A) and *bc* (B) planes. C: DSC plot showing a weak first order phase transition at about T = 340 K. D: Thermal expansion of the volume as measured by XRD (inset: zoom near the transition zone). E. Evolution of the bond lengths across the transition. F and G: Evolution with temperature of the anisotropic displacements parameters U11, U22 and U33 of PbO2 and O1 atoms.

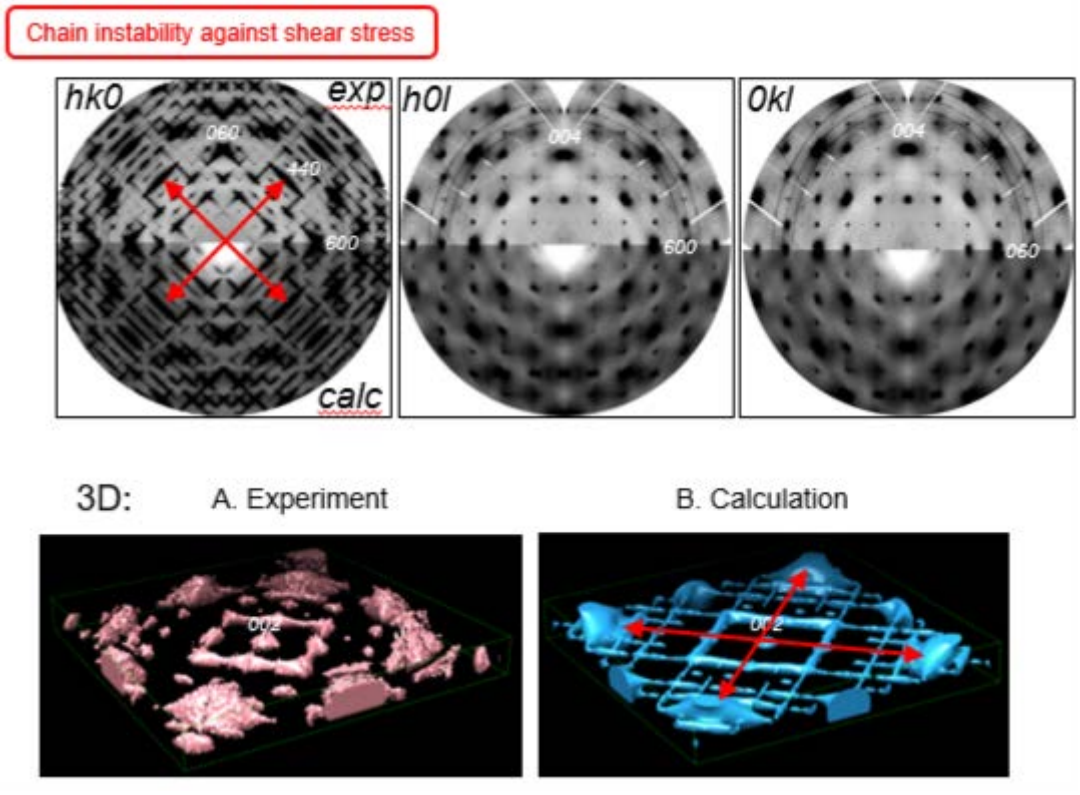

Figure 3. 2D maps (top): reconstructed *hk0, h0l* and *0kl* reciprocal space maps of Pb_2SnO_4 (top panels) versus calculated maps (bottom panels), showing the good agreement between measured TDS and the *ab-initio* phonon calculations. 3D maps (bottom): experimental (red) and calculated (blue) *hk2* planes.

3. Soft-phonon driven phase transition in $BaVS_3$

At ambient conditions $BaVS_3$ crystalizes in a hexagonal structure with space group $P6_3/mmc$ and lattice parameters a = 6.719 Å, and c = 5.619 Å. Its structure consists of chains of V–S face sharing octahedra running in the c-direction and separated by Ba. At T_S = 240 K, the crystal symmetry is lowered from hexagonal to orthorhombic through a displacive second order phase transition associated with a zigzag deformation of the V-S chains. The transition has been long thought to be driven by the softening of a phonon, but the soft mode could never be observed experimentally. Here we used combined diffuse scattering, inelastic X-ray scattering and ab initio calculations to experimentally and theoretically confirm the soft mode character of the symmetry lowering at T_S. 3D reconstruction of the diffuse signal around 301 reflection far above (T = 330 K), just above (T = 260 K) and below T_S (T = 200 K) are gathered in Figure 4 A, B and C respectively. Upon approaching the transition, a strong diffuse signal appears centered at the Γ point and disappears below the transition, indicating the softening of a zone-center phonon. The lattice dynamics with temperature was further investigated by IXS around q = (3.1,0,1). The dispersion of the soft mode was measured above T_S (Fig. 4D), and its softening is evidenced by the large variation of the central peak upon approaching the transition (Fig. 4E). Combined TDS and IXS experiments allowed to identify the soft mode as a low energy optical mode, while Raman experiments did not allow its observation. Analysis of the DFT calculations is ongoing to identify the soft mode.

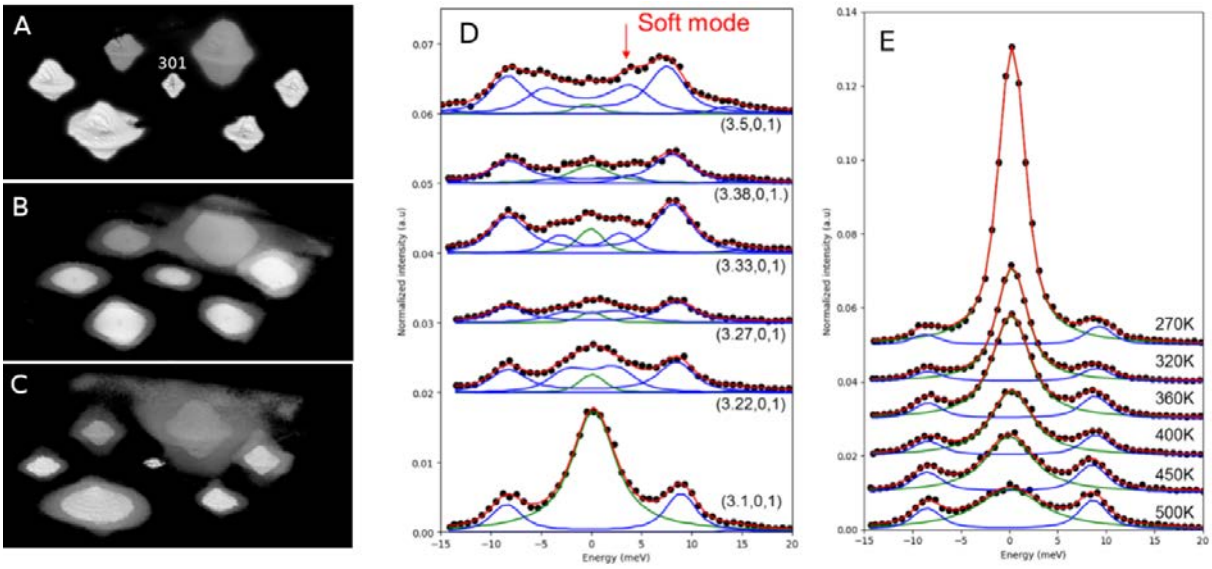

Figure 4. A, B, C: TDS signal around 301 reflection far above (T = 330 K), just above (T = 260 K) and below T_S (T = 200 K). D: Dispersion of the soft mode measured by IXS. E: Temperature dependence of the soft mode across the transition.

4. Lattice dynamics of $CaCO_3$ and $MgCO_3$

Calcium and magnesium carbonates are the most abundant carbonates on Earth. They are present in oceanic sediments, from where they can be transported to the Earth interior on subducting slabs.

Understanding the physical properties of these carbonates is a key to understand and detect the processes responsible for transportation of carbon into the deep Earth. The lattice dynamics of these compounds govern the thermodynamic and transport properties, from which geoscientifically important parameters can be derived, such as sound velocities, bulk moduli, thermal expansion and thermal conductivity.

We performed x-ray scattering experiments at ID28 at the ESRF. The side station diffractometer was used to obtain diffuse scattering maps of $CaCO_3$ and $MgCO_3$ at ambient conditions (Fig. 5). As has been observed by Dove et al. before, there is strong diffuse scattering in $CaCO_3$ at the F point of the Brillouin zone (Fig. 5A). We did not observe such features for $MgCO_3$. Further measurements were conducted with the inelastic x-ray scattering spectrometer. We measured the phonon dispersion relations of $CaCO_3$ and $MgCO_3$ in the Γ-F direction. We have observed strong softening of the quasi-transverse acoustic phonon in the case of $CaCO_3$ (Fig. 6A), responsible for the high intensity signal in the diffuse scattering maps. We didn't observe any softening at the F point in the case of $MgCO_3$ (Fig. 6B).

The observed difference in the lattice dynamics may lead to an explanation of the difference in the stabilities of $CaCO_3$ and $MgCO_3$. The IXS and diffuse scattering data and their interpretation will be presented during the 26th DGK meeting, a corresponding article is in preparation.

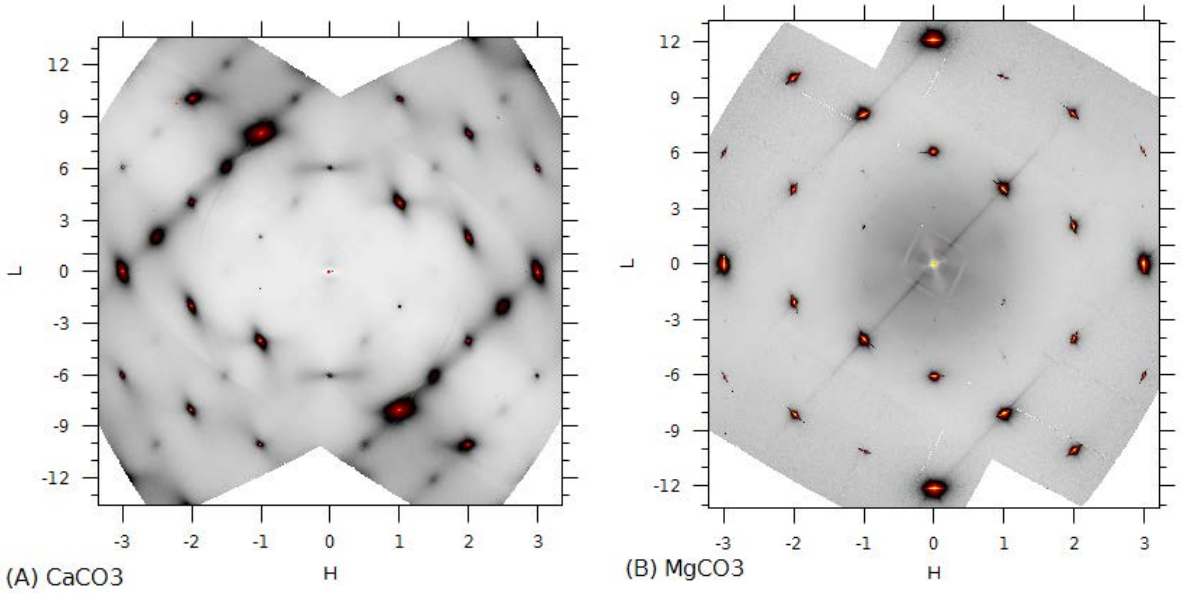

Figure 5. Diffuse scattering maps of $CaCO_3$ (A) and $MgCO_3$ (B) in the (H 0 L) plane of the reciprocal space. Strong intensity is observed in the (-2.5 0 2) and (-1.5 0 6) points, that correspond to the F in the Brillouin zone of $CaCO_3$. These features were not observed in the case of $MgCO_3$.

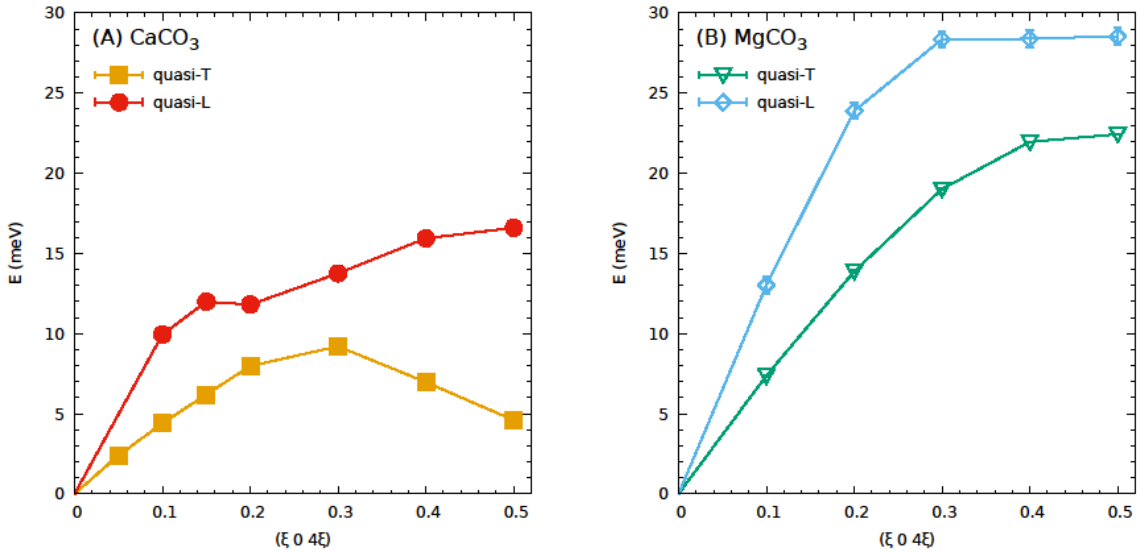

Figure 6. Phonon dispersion relations of $CaCO_3$ (A) and $MgCO_3$ (B) of the quasi-longitudinal (quasi-L) and quasi-transverse (quasi-T) acoustic modes along Γ-F direction. The quasi-transverse acoustic mode in $CaCO_3$ softens in the vicinity of the F point at ξ= 0.3. Such a behaviour is not observed in the case of $MgCO_3$. Errors are smaller than the symbol size.

5. High temperature measurements in the diamond sample chamber

The aim of the experiment was to investigate the lattice dynamics of carbonates at elevated temperatures, above their decomposition temperature. In order to prevent the decomposition of the sample at high temperatures it needs to be kept in a CO_2 atmosphere at elevated pressure. A novel high temperature cell suitable for such experiments is depicted in Fig 7. As carbon dioxide is highly reactive at high temperatures, the sample chamber consists of two opposing diamonds, as this is one of the few materials that does not react with CO_2 at such conditions. The diamond assembly is heated via a resistive heating system, and pressed uniaxially in order to confine the CO_2 inside the diamond chamber. The diamond assembly is kept in vacuum in order to avoid an oxidization of diamond at high temperatures.

We have first commissioned and tested the new diamond sample chamber offline, and proceeded with the measurement at ID28 during the LTP beamtime. The sample used was a single crystal of calcite, $CaCO_3$, cut and polished in a plate shape, so that the momentum transfer vectors in the (H0L) plane were accessible for the measurement. The crystal was glued to the bottom of the chamber with MgO cement. The diamond chamber was sealed by putting graphite rings in the conical part of the upper diamond. A few grains of $MgCO_3$ powder, which has a lower decomposition temperature than $CaCO_3$, were put aside the crystal to produce CO_2 inside the chamber.

We have performed three experimental runs with the assembly. In the first one the amount of $MgCO_3$ powder was too large. The CO_2 pressure was much higher than the uniaxial stress exerted by the sample environment equipment, so that a leak in the diamond chamber was observed along with the loss of pressure and sample decomposition. In the second run we observed the leak of oil in the hydraulic system used to pressurize the diamond assembly, which again resulted in loss of pressure in the sample chamber. After fixing the oil leak we performed the third run, and again observed the sample decomposition. The cause was interpreted to be a CO_2 leak through the graphite sealing rings. After minor modifications further experiments at ID28 with improved equipment are planned for the

first semester of 2018. We plan to seal the diamond chamber with additional outer gold rings, which plasticity should prevent any leak in the chamber.

A) **B)**

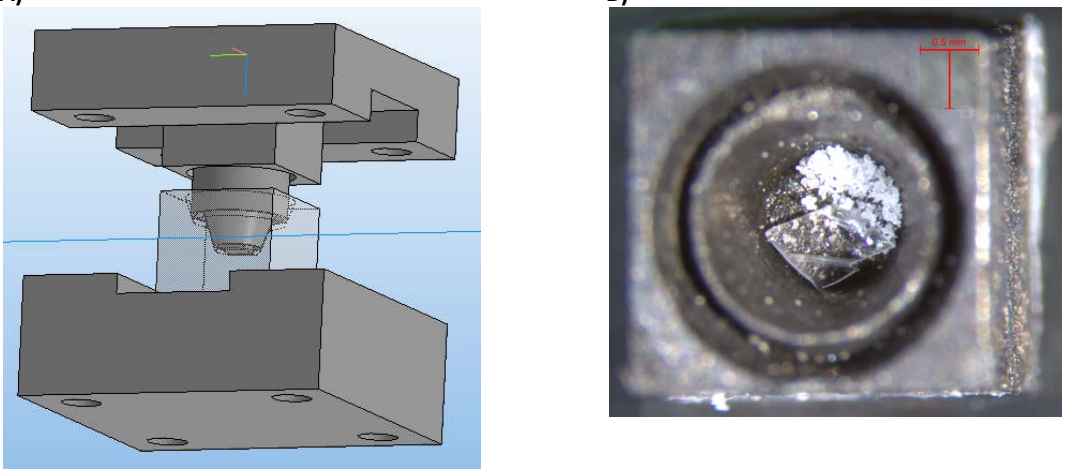

Figure 7. A) Diamond sample chamber assembly with a bulk diamond cut in two pieces: one with a hole (transparent part), and a second one with conical top (solid part on top of the transparent part). The diamonds are placed in graphite holders (topmost and bottommost parts) used to position the sample in the center of the assembly, prevent a movement of the diamonds and ensure a proper thermal contact with the heaters. B) Bottom part of the diamond assembly, with the transparent calcite crystal and white $MgCO_3$ powder used for the experiment.

6. Lattice dynamics of low temperature WO_3 phases

We have studied the lattice dynamics of tungsten trioxide as a function of temperature (160 K < T < 350 K) by high resolution inelastic x-ray scattering, IXS, and diffuse scattering, DS. The crystal structure of WO_3 can be described as a distorted ReO_3 structure, where the WO_6-octahedra are corner-connected. At 300 K WO_3 is monoclinic, at 290 K it transforms to a triclinic structure and at 230 K to another monoclinic structure. The distortion of WO_6-octahedra increases with decreasing temperature. Kawaminami and Hirose (1979) suggested that the phase transitions are due to a condensation of phonons at the Γ, M and R points of the cubic aristotype.

We have measured diffuse scattering maps at the side station of ID28 at ESRF. At 350 K and 250 K we have observed strong diffuse scattering around the (4 0 0) Bragg reflection in the form of diffuse planes, with the normal being the (1 0 0) vector in reciprocal space. This is consistent with our predictions based on DFT calculations. However, at 165 K, where WO_3 is in the low temperature monoclinic phase, the diffuse planes are less pronounced compared to the higher temperature phases, see Fig. 8. DS measurements helped us to choose the most promising regions for an IXS study on ID28. We have measured the acoustic phonon spectra at 400 K, 290 K, 270 K and at 160 K along the main crystallographic directions.

The data analysis is currently ongoing, the focus is to compare the results of the calculations with the DS and IXS measurements and identify the soft phonons. Partial results of this study were presented on the IXS-2017 conference in Hamburg, Germany.

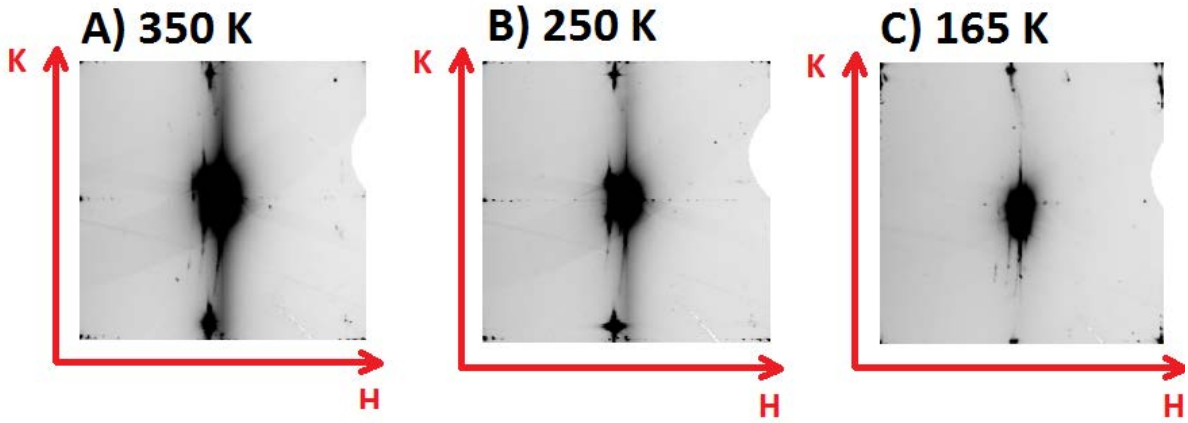

Figure 8. Diffuse scattering signal of WO_3 around the (4 0 0) reflection in the (H K 0) plane. The diffuse signal forms diffuse planes with the normal parallel to the (1 0 0) vector in reciprocal space. The diffuse plane intensity is decreasing in the consecutive low temperature phases of WO_3: monoclinic (A), triclinic (B) and low-T monoclinic (C).